Available online at www.sciencedirect.com
SCIENCE DIRECT®
Earth and Planetary Science Letters 240 (2005) 307–321
EPSL
www.elsevier.com/locate/epsl

Seasonal seismicity at western United States volcanic centers

L.B. Christiansen [a,*], S. Hurwitz [a], M.O. Saar [b], S.E. Ingebritsen [a], P.A. Hsieh [a]

[a] U.S. Geological Survey, Menlo Park, CA 94025, United States
[b] University of Minnesota, Dept. of Geology and Geophysics, Minneapolis, MN 55455, United States

Received 23 March 2005; received in revised form 26 August 2005; accepted 13 September 2005
Available online 25 October 2005
Editor: R.D. van der Hilst

Abstract

We examine 20-yr data sets of seismic activity from 10 volcanic areas in the western United States for annual periodic signals (seasonality), focusing on large calderas (Long Valley caldera and Yellowstone) and stratovolcanoes (Cascade Range). We apply several statistical methods to test for seasonality in the seismic catalogs. In 4 of the 10 regions, statistically significant seasonal modulation of seismicity (>90% probability) occurs, such that there is an increase in the monthly seismicity during a given portion of the year. In five regions, seasonal seismicity is significant in the upper 3 km of the crust. Peak seismicity occurs in the summer and autumn in Mt. St. Helens, Hebgen Lake/Madison Valley, Yellowstone Lake, and Mammoth Mountain. In the eastern south moat of Long Valley caldera (LVC) peak seismicity occurs in the winter and spring. We quantify the possible external forcing mechanisms that could modulate seasonal seismicity. Both snow unloading and groundwater recharge can generate large stress changes of >5 kPa at seismogenic depths and may thus contribute to seasonality.

Keywords: seasonality; earthquake triggering; pore-fluid pressure; seismic activity; volcano

1. Introduction

Considerable progress has been made during the past several decades toward better understanding of volcanic processes and mitigating volcano hazards. Much of this progress has been achieved by increasing the density and sophistication of seismic networks in active volcanic areas. Patterns of seismicity in the western United States following large and remote earthquakes suggest that triggered seismicity is more likely to occur in the relatively hot, weak crust of volcanic areas [1–3]. Several mechanisms have been proposed to explain this phenomenon including rectified diffusion [4], changes to the state of fault surfaces from dynamic stresses of mainshock events [5], changes to the state of magma bodies caused by dynamic stresses from a distant earthquake [6,7], and fluid pressure variations in pores and fractures as large seismic waves pass through a region [8–10]. Further, Gao et al. [11] found that in parts of California the timing of earthquakes was annually modulated for 5 yr following the magnitude 7.3 Landers earthquake, with more earthquakes occurring in the latter half of the year, especially in hydrothermal and volcanic areas. They concluded that the annual pattern is probably induced by an external stress, possibly barometric pressure variations.

Other studies have suggested that seismicity in both continental volcanoes and sub-seafloor hydrothermal systems can be modulated by daily Earth tides [12–

* Corresponding author. Tel.: +1 650 329 4420; fax: +1 650 329 4538.
E-mail address: lchristi@usgs.gov (L.B. Christiansen).

0012-821X/$ - see front matter © 2005 Elsevier B.V. All rights reserved.
doi:10.1016/j.epsl.2005.09.012

14] and by climatic forces that have an annual period [15–18]. The suggestion that large-scale, global climatic forcing may influence seismic activity [19,20] is of particular interest because it suggests that volcano hazard assessment and monitoring efforts should take into consideration both seasonal and long-term climate variability.

In studies of volcanic areas where seasonal seismicity has been detected, the maxima in seismic activity appear to occur 1 to 6 months after the majority of snowmelt [15,17,18]. Based on this lag period, it has been proposed that the earthquake triggering mechanism is diffusion of pore pressure to the earthquake nucleation zone several kilometers beneath the volcano [17,18]. This mechanism is feasible under a narrow but plausible range of permeabilities, porosities, and water saturations. It has also been suggested that unloading of the snow pack is the mechanism for triggering earthquakes [15]. Since elastic rheology would imply that earthquakes should occur instantaneously following removal of the snow load, Heki [15] proposed that the lag time between snowmelt and seismicity represents the earthquake nucleation time, with larger delay periods expected for larger earthquakes.

In this study, we explore the extensive available data sets from active volcanic systems in the western United States, including stratovolcanoes of the Cascade Range and the large calderas at Yellowstone and Long Valley (Fig. 1). The regional tectonism in these areas provides the close-to-critical background stress necessary to allow seasonal triggering of seismicity. We apply a variety of statistical tests to the data sets to determine which systems (if any) have seasonal trends in seismicity, presumably modulated by external climatic forcing. We then discuss possible mechanisms to explain annual periodicity in seismic records.

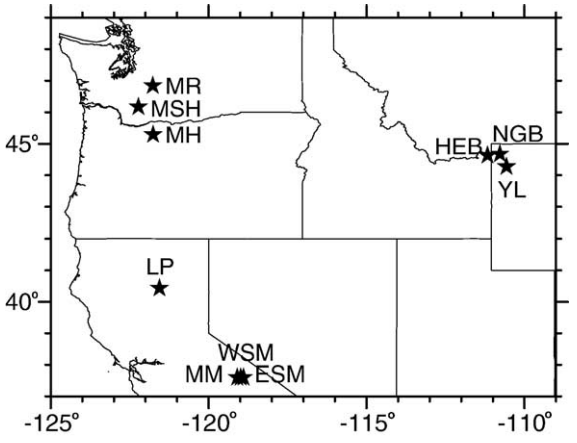

Fig. 1. Location map of study areas in the western USA: MR=Mt. Rainier, MSH=Mt. St. Helens, MH=Mt. Hood, LP=Lassen Peak, ESM=eastern south moat, WSM=western south moat, MM=Mammoth Mountain, HEB=Hebgen Lake/Madison Valley, NGB=Norris Geyser Basin, YL=Yellowstone Lake.

2. Study areas

We investigate 10 volcanic systems in the western United States characterized by frequent seismicity: four stratovolcanoes in the Cascade Range (Mt. St. Helens, Mt. Hood, Lassen Peak, and Mt Rainier) and six seismically active subareas at LVC and Yellowstone (Fig. 1). Each of the selected areas has at least 20 yr of available seismic records. In order to have meaningful statistical analyses, areas were only examined if there were at least 50 earthquakes with magnitudes greater than the minimum requirement for catalog completeness. Other volcanic areas such as Mt. Adams, Mt. Bachelor, Mt. Baker, Glacier Peak, and Mt. Shasta were excluded from the analysis because the seismic catalogs do not span long enough periods, are incomplete, or do not have a sufficient number of earthquakes during the 20-yr period of this study.

2.1. Cascade range

The Cascade Range extends approximately 1200 km from southern British Columbia to northern California. It is located on a tectonically active, convergent plate boundary between the North American and Juan de Fuca plates, and has been volcanically active for about 40 million yr. Several major Quaternary stratovolcanoes are in close proximity to populated regions, making it especially important to understand their seismic behavior.

We analyzed seismic patterns from four volcanoes that have sufficient data to support statistical analysis: Mt. St. Helens and Mt. Rainier in Washington, Mt. Hood in Oregon, and Lassen Peak in California (Fig. 1). Most seismic events in these four areas occur at relatively shallow depths. At Mt. St. Helens, most of the seismicity extends to depths of ~9 km below the mean station elevation, although there is a zone of concentrated seismicity that occurs at a depth of ~3 km [21]. At Mt. Rainier, most of the seismicity occurs in the upper 3 km of the crust [22]. The seismicity at Mt. Hood is more evenly distributed between the mean station elevation and a depth of 7 km [23]. At Lassen Peak, most of the seismicity occurs at depths of approximately 3–5 km [24]. Seismic records in Washington and Oregon are available through the Pacific Northwest Seismic Network (http://www.geophys.

washington.edu/SEIS/PNSN/), and data from Lassen Peak are obtained from the Northern California Earthquake Data Center (http://quake.geo.berkeley.edu).

2.2. Long Valley caldera

Long Valley caldera (LVC) is a 450-km^2 elongated depression located at the boundary between the Sierra Nevada and the Basin and Range provinces (Fig. 1). Cenozoic volcanism began approximately 3.6 to 3.0 Ma ago in response to Basin and Range extension [25]. Approximately 0.7 Ma ago, an eruption of 600 km^3 of rhyolitic material caused the roof of a magma chamber to collapse and created the present-day caldera [26]. LVC has an active hydrothermal system, including hot springs, fumaroles, and mineral deposits [27].

LVC is extensively monitored, with a dense network of 18 seismic stations within the caldera and an additional 20 stations within 50 km of the caldera boundary. These stations are operated by the Northern California Seismic Network and the Nevada Seismic Network (http://quake.geo.berkeley.edu). Over the past 20 yr, most seismic activity has occurred in the south moat region of LVC [9]. Two seismically active regions of the south moat are separated by a narrow aseismic gap. For the statistical analyses, we separate the south moat into two subareas following this natural divide in seismicity. We also examine the pattern of seismicity at Mammoth Mountain, located outside the structural rim of the caldera west of the south moat. Seismic activity in this area is significantly shallower (depths of 3–7 km below mean station elevation) than in the south moat (depths of 5–10 km).

2.3. Yellowstone National Park

Yellowstone National Park and its surroundings (Fig. 1) are part of the Yellowstone plateau volcanic field that spans parts of Wyoming, Idaho, and Montana. The Yellowstone area is the most recent surface expression of a migrating, 17-million-yr-old volcanic center that can be tracked through southwestern Idaho. Three large Quaternary caldera-forming rhyolitic eruptions occurred in Yellowstone, the last occurring at 0.64 Ma [28]. At that time, an eruption formed the present-day caldera, which consists of two overlapping ring-fracture zones that form a topographic basin 85 by 45 km. Subsequently, smaller eruptive events occurred inside and around the caldera [28].

The Yellowstone Seismic Network comprises more than 20 seismometers located in and around the National Park (http://www.seis.utah.edu/catalog/ynp.shtml). Seismicity is concentrated in the western part of the Park, although it occurs throughout the caldera [29]. Earthquakes are generally confined to the upper 10 km of the crust.

We analyzed the seismicity in three regions of Yellowstone that are relatively well instrumented: (1) The Hebgen Lake/Madison Valley area in the northwestern portion of the Park, which had a major earthquake (M=7.5) in 1959 [30]; (2) Norris Geyser Basin, east of Madison Valley; and (3) Yellowstone Lake, in the southeast portion of the caldera, which hosts abundant hydrothermal activity [31].

3. Methodology

Our analyses are based on 20 yr of seismic data extending from January 1, 1984 to January 1, 2004. The density of the seismic arrays varies between locations, which affects the completeness of each seismic catalog. To ensure that measurement bias caused by station density and location does not affect the results of the statistical analyses, we examined a frequency–magnitude distribution for the earthquake sequences, as represented by b-values in the Gutenberg–Richter relationship:

$$\log_{10}N = a - bM \quad (1)$$

where N is the cumulative number of earthquakes with a magnitude M and a is a constant representing the rate of seismic productivity for a given localized area. Main shock–aftershock sequences typically yield b-values of 1, whereas values less than 1 represent a loss of lower-magnitude earthquakes, possibly due to lack of instrument sensitivity and/or density. We use b=1 in the Gutenberg–Richter relationship to determine the minimum magnitude for completeness in the catalog, and exclude earthquakes with smaller magnitudes from the analysis (Fig. 2), whereas all earthquakes with greater magnitudes are included. In LVC, where there is a dense seismic network, we use a minimum magnitude of M=1; in the Cascade Range, we use a minimum magnitude of M=1.5; and in Yellowstone National Park, we use a minimum magnitude of M=2.

Seismometer malfunctions in the study areas may cause a bias toward increased seismicity during the summer because the stations tend to fail more often in the winter, due to storms, and because outages during the winter months tend to last longer, due to access difficulties. Excluding the smallest earthquakes (below the given magnitude cutoff for catalog completeness) makes it more likely that our results are not affected by this bias. Additionally, the limited data regarding the

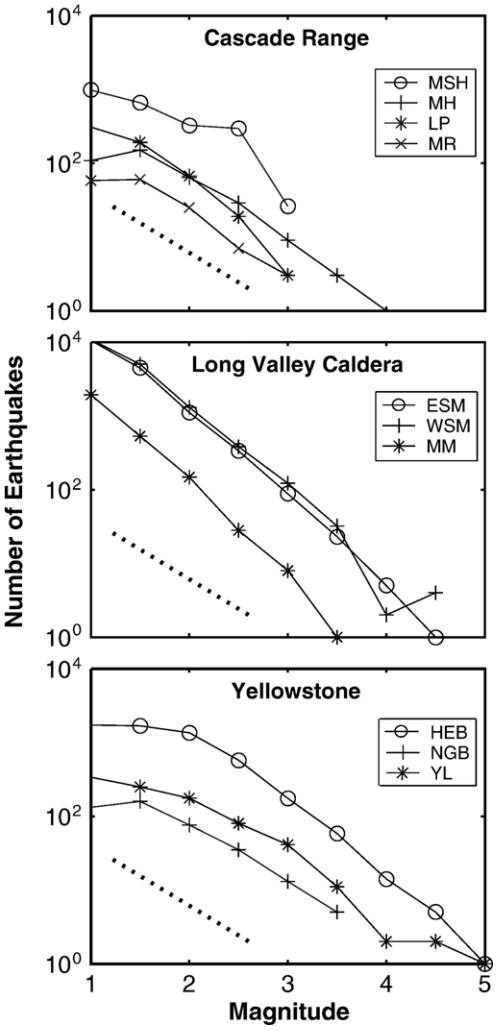

Fig. 2. Magnitude versus logarithmic frequency of earthquakes (Gutenberg–Richter relationship) for each study area. Magnitude is binned by half-magnitude increments. Dotted lines plot $b=1$. Minimum magnitudes used to ensure complete earthquake catalogs are $M=1$, 1.5, and 2 for Long Valley caldera, the Cascade Range, and Yellowstone, respectively. Abbreviations are the same as in Fig. 1.

timing of seismometer outages seem to indicate that not all seismic stations for a given area fail at the same time. To examine this possible bias quantitatively, we used a frequency–magnitude plot for 3-month intervals during the year (January through March, April through June, etc.). In these analyses, the minimum magnitude is the same as that of the full data set.

Information based on the cumulative seismic moment can also help identify seasonal patterns by showing whether large earthquakes occur during the same period as the highest frequency of earthquakes. We calculate the cumulative seismic moment, (M_0), defined as $M_0 = 10^{1.5(M+10.73)}$, for each month and apply the same methodology as used for the number of earthquakes. Results for the seismic moment will more likely be dominated by the (few) larger earthquakes, whereas the total number of earthquakes emphasizes smaller, frequent earthquakes where a seasonal signal would more likely reside. By examining both types of information, we can determine whether more frequent and larger earthquakes tend to occur during the same time period.

Seismic events are binned monthly for each data set. We then group the data into 2-month, 3-month, and 6-month groups and use statistical analyses to determine whether the number of earthquakes per month for months in a given group over the 20-yr period is different than that for other groups. We apply ANOVA and Kruskal–Wallis (H test) variance tests [32] and the Schuster Random-Walk test [33,34] to each group and require a probability of 90% (p-value ≤ 0.10) for statistical significance. Groups are rotated throughout the year (i.e. January through June, February through July, March through August, etc.), such that we find the most statistically significant period of elevated seismicity. Earthquake sequences and the test results for 6-month groupings are summarized in Tables 1 and 2.

An ANOVA test compares the variances within two or more populations to determine if the means of the groups are statistically different. By using the variances, the test can determine if the difference between populations is due to random error (as would be detected by the variance) or by a true difference in means. In the case where an ANOVA test is applied to only two populations (such as the case with 6-month groups), it gives the same results as a Student's t-test. One assumption inherent in an ANOVA test is that the variances in the sample populations are small. In the analyzed data, variances between groups can be quite large. We apply three methods of normalization to transform data and reduce the variances before ANOVA tests are performed, and compare the results to those obtained using non-normalized data. Data transformation is a process by which the original scale of measurement is converted to a new scale. In the first two methods, data are transformed using square-root and logarithmic functions, both traditional methods for normalizing data. In these two methods, either the square root or the logarithm, respectively, of the number of earthquakes per month is used in the ANOVA test as opposed to the original value [32]. The square-root method is ideal for cases where means are approximately proportional to the variances of their respective means. The logarithmic transformation is

Table 1
Results of statistical analyses

Location	Number of earthquakes	A	A_{sqrt}	A_{log}	A_{yr}	K–W	Sch.	Seasonal ?
Cascades								
Mt. St. Helens	1306	0.20	**0.05**	**0.04**	**0.02**	**0.03**	0.27	✓
Mt. Hood	187	0.30	0.49	0.32	0.33	0.32	**0.02**	
Lassen Peak	154	0.22	0.25	0.20	**0.10**	0.25	0.15	
Mt. Rainier	63	0.21	0.19	0.13	0.22	0.13	**0.07**	
Long Valley								
Eastern south moat	16558	**0.06**	**0.10**	0.17	**0.05**	0.18	<**0.001**	✓
Western south moat	17768	0.12	0.23	0.25	**0.004**	0.28	<**0.001**	
Mammoth Mountain	2650	**0.05**	**0.03**	**0.03**	**0.002**	**0.007**	<**0.001**	✓
Yellowstone								
Hebgen L./Madison V.	1967	0.15	0.32	0.60	0.17	0.69	<**0.001**	
Norris Geyser Basin	161	0.28	0.28	0.21	0.37	0.18	**0.04**	
Yellowstone Lake	497	**0.01**	**0.003**	**0.02**	**0.01**	**0.02**	0.20	✓

A=ANOVA, A_{sqrt}=ANOVA with a square-root normalization, A_{log}=ANOVA with a logarithmic normalization, A_{yr}=ANOVA with yearly normalization, K–W=Kruskal–Wallis, and Sch.=Schuster Random Walk. Significant values are in bold. Results are for 6-month binning. Regions where data show convincing evidence for seasonality are identified in the last column.

Table 2
Results for regions that show seasonality in three out of five tests (excluding Schuster tests) for 2- and 3-month binning, for cumulative seismic moment (6-month binning), and for the top 3 km of the crust only

Location	A	A_{sqrt}	A_{log}	A_{yr}	K–W
Full data set					
3-month					
Yellowstone Lake	**0.04**	**0.02**	0.11	**0.06**	0.11
2-month					
Mt. St. Helens	0.30	0.31	**0.04**	**0.01**	**0.04**
Yellowstone Lake	**0.05**	**0.04**	0.23	**0.06**	0.19
Cumulative Seismic Moment (6-month)					
Mt. St. Helens	**0.10**	**0.05**	**0.07**	**0.08**	**0.08**
Eastern south moat	**0.04**	**0.02**	**0.07**	**0.02**	0.18
Mammoth Mountain	0.16	**0.07**	**0.04**	**0.04**	**0.005**
Yellowstone Lake	**0.08**	**0.03**	**0.04**	**0.05**	**0.03**
Top 3 km					
6-month					
Mt. St. Helens	0.19	**0.06**	**0.04**	**0.01**	**0.05**
Eastern south moat	**0.05**	**0.08**	**0.09**	**0.07**	0.21
Mammoth Mountain	**0.06**	**0.01**	**0.006**	**0.002**	**0.004**
Hebgen L./Madison V.	**0.04**	**0.06**	**0.09**	**0.03**	**0.08**
Yellowstone Lake	**0.04**	**0.001**	**0.001**	**0.001**	**0.002**
3-month					
Eastern south moat	**0.03**	**0.06**	0.16	**0.01**	0.27
Mammoth Mountain	0.17	**0.05**	**0.04**	**0.01**	**0.04**
Hebgen L./Madison V.	**0.02**	**0.04**	**0.02**	**0.005**	**0.01**
Yellowstone Lake	**0.05**	**0.003**	**0.008**	**0.003**	**0.01**
2-month					
Mammoth Mountain	0.28	**0.10**	**0.10**	**0.02**	**0.09**
Hebgen L./Madison V.	0.11	0.11	**0.07**	**0.03**	**0.05**
Yellowstone Lake	**0.10**	**0.01**	**0.03**	**0.004**	**0.05**

Abbreviations are the same as in Table 1. Significant values are in bold.

appropriate if means are proportional to the range or standard deviation of respective means. The third method for normalizing data specifically addresses interannual variability in the amount of seismicity, such as might be associated with magmatically or tectonically driven seismicity. For each year analyzed, we divide the number of earthquakes for each month by the maximum monthly total for that year, so that the monthly number of earthquakes may vary between 0 and 1. Each year is normalized independently. With this normalization method, each year has the same weight as other years in the analysis. Thus, a year with many earthquakes does not dominate the pattern. Because a large number of measurements are needed before any definite conclusion can be made about the most appropriate transformation, we compare all three methods to ensure that the transformations are not altering the end results.

The Kruskal–Wallis test is a rank-sum method that determines if random samples come from identical populations. By ranking the data instead of using the raw values, assumptions about the distributions of the populations are unnecessary. Therefore, we do not need to transform the data to use this test.

The Schuster Random Walk test has been applied in previous studies to assess periodic signals in seismicity (e.g. [13,14,35]). In this test, each seismic event is given a unit length and assigned an angle from 0° to 360°, depending on the day of the year (January 1 is given an angle of 0°). Each vector is plotted sequentially, tail to head, to create a random walk line depicting the timing of events. As the distance of the random

walk line from the origin increases, the probability for a non-uniformly distributed population increases. The path of the random walk line shows the sequential timing of earthquake events throughout the course of time series. A randomly distributed population will produce an average walkout length with a radius of $R = 0.5\sqrt{\pi N}$ from the origin. The Schuster test provides an expression for determining the probability, P_{rw}, that a randomly distributed population would exceed R, based on the distance of the random walk, D, for a given number of events, N:

$$P_{rw} = \exp\left(-D^2/N\right). \quad (2)$$

If the end distance of the random walk exceeds a certain probability, the null hypothesis of random event phases can be rejected and the population may contain a nonrandom component [33,34].

In many cases, close examination of Schuster test results reveals that one or more years dominate the random walk pattern, due to elevated levels of seismicity as compared to more typical years. The high-seismicity periods, likely caused by either magma intrusions or tectonic activity and unrelated to seasonal patterns, are classified as swarm periods. We develop a method to remove these periods from the catalog for each location (Appendix A). The seismic moment, which has both an angular vector (determined by the date) and a magnitude (determined by the moment), cannot be examined using a Schuster test. Another drawback of this test is that it may tend to overestimate the significance of the results [36]. Under some circumstances, it can also underestimate seasonality: as years of data are removed during deswarming, the length of the time series is reduced, decreasing the statistical significance.

4. Results

Data from 4 of the 10 regions show a statistically significant increase in monthly seismicity during a given time of the year, hereafter referred to as seasonality (Table 1). Results from the different statistical tests did not agree in all cases, and we consider statistical significance of $\geq 90\%$ in four of the six tests to be convincing evidence of seasonality. When data were grouped by 2- or 3-month groups, a statistically significant period of increased seismicity was not detected in any of the regions. However, at Yellowstone Lake, 2- and 3-month groups display seasonality in three of the six tests. In data from Mt. St. Helens, three of six tests indicate seasonality in 2-month groups, but not 3-month groups. The remainder of the discussion will refer to 6-month groups unless otherwise stated. Test results based on the cumulative monthly seismic moment show similar results to those that examined the number of earthquakes (Table 2).

Certain statistical tests tend to overestimate the likeliness of seasonality. In particular, Schuster tests results indicate a non-random component in the distribution of earthquakes in 7 of the 10 regions, often in conflict with all other tests. In addition, data from some regions which prove to have a seasonal component based on ANOVA or Kruskal–Wallis tests are not identified using the Schuster test methodology. For two locations, yearly normalization appears to overstate the significance of seasonality as compared to the other tests. Other methods for data transformation, and the non-normalized data, all generally provided similar results, although sample population variances were high in the non-normalized and square-root transformation methods. We conclude that the best approach to assessing seasonality is to apply several statistical tests side by side in order to generate robust, plausible results.

In the Cascade Range, Mt. St. Helens is the only volcanic area where data show convincing evidence for seasonal seismicity. Four of the six statistical tests (ANOVA with square root, logarithmic, and yearly normalization, and the Kruskal–Wallis test) indicate elevated seismicity during May through November (Table 1; Fig. 3). p-Values range from 0.02 in the ANOVA test with yearly normalization to 0.05 in the ANOVA test with a square root transformation. The ANOVA test without normalization and the Schuster test do not indicate any trends in the timing of earthquakes. The cumulative seismic moment at Mt. St. Helens increases from May through December in all five statistical tests (p-values ranging from 0.05 to 0.10), consistent with the results based on the number of earthquakes. In the other three volcanic areas in the Cascades, statistical significance was met in only one of the six tests, leading us to believe that there is no detectable seasonal pattern to earthquake timing and magnitude. In contrast to an earlier study exploring seasonality at Mt. Hood [17], our statistical analyses do not indicate seasonality there. This difference may be due to their data preprocessing and relatively short time series for use in power spectra, while we focus on a variety of standard statistical techniques of unprocessed data with comparison to normalized time series. We calculate power spectra of unprocessed data from areas with seasonal seismicity (discussed later) for comparison to other studies.

In LVC, data from both Mammoth Mountain and the eastern south moat region show seasonal modulation of

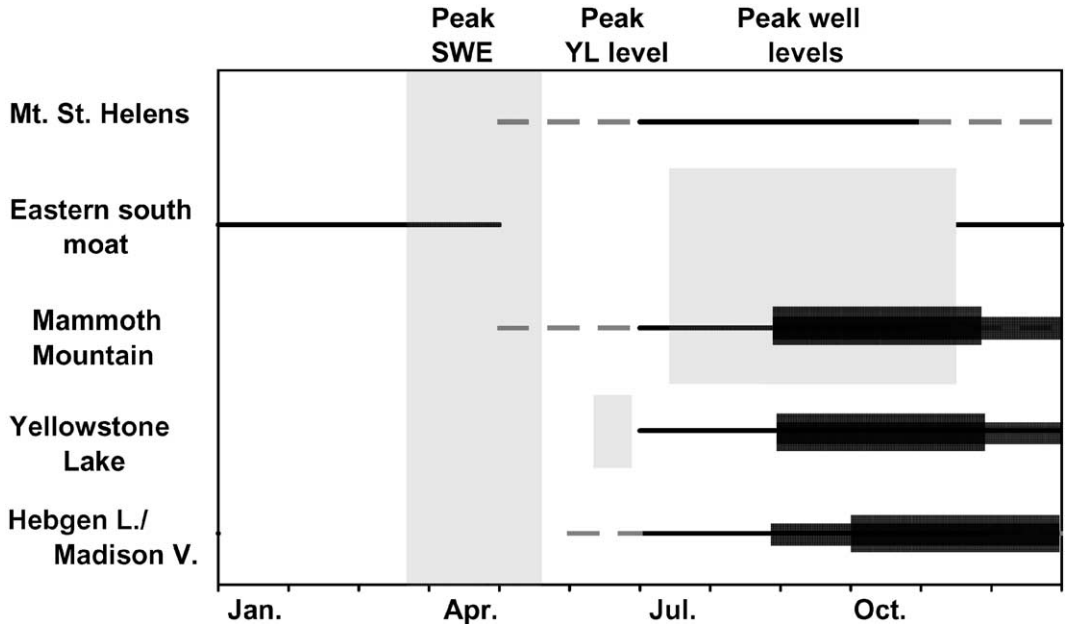

Fig. 3. Timing for elevated seismicity for each region that has statistically significant seasonality. For the Hebgen Lake/Madison Valley region, we use data from only the upper 3 km of the crust. The timing varies depending on the statistical test. The bold line represents the time interval that coincides in all statistical tests, whereas the grey dashed line shows the possible extent of increased seismicity based on individual tests. Shaded grey areas show timing of peak snow water equivalent (SWE), peak lake level at Yellowstone Lake (YL), and peak water table levels based on well data from Long Valley caldera. Thicker lines for Mammoth Mountain, Hebgen Lake/Madison Valley, and Yellowstone Lake show timing for 2- and 3-month periods of elevated seismicity in the top 3 km of the crust only.

seismicity. At Mammoth Mountain, all six statistical tests indicate significance, with p-values ranging from <0.001 (Schuster) to 0.05 (ANOVA). Increased seismicity occurs from approximately May through December, depending on the test. Seasonality in the cumulative seismic moment is significant in four of the five analyses (p-values range from 0.005 to 0.07, excluding ANOVA). The timing of the elevated seismic moment coincides with that of the elevated number of earthquakes. In the eastern south moat, four of the six tests indicate significant seasonality (p-values range from <0.001 to 0.10, excluding ANOVA with logarithmic normalization and Kruskal–Wallis). Seismicity is elevated from October to May. The cumulative seismic moment also increases during October through May, with p-values ranging from 0.02 to 0.07, excluding Kruskal–Wallis. In the western south moat, there is evidence for non-randomly distributed seismicity in the ANOVA test with yearly normalization and the Schuster test. However, because the other tests do not show indications of increased seismicity during a portion of the year, we conclude that seasonal seismicity cannot be confirmed in this region.

At Yellowstone, Yellowstone Lake has elevated seismicity from July through December. This period is coincident with a period of lake level drop (http://volcanoes.usgs.gov/yvo/LakeLevelData1990-2003.txt). The increase in seismic activity is statistically significant in five of the six tests (p-values range from 0.003 to 0.02, excluding Schuster). Cumulative seismic moment is also elevated from July through December (p-values range from 0.03 to 0.08). Three statistical tests (ANOVA and ANOVA with square root and yearly normalization) show increased seismicity in both 2- and 3-month groups. The 2-month period of increased seismicity occurs between September and November, depending on the test. The 3-month period of increased seismicity occurs between September and December, again depending on the test. The data from Norris Geyser Basin and Hebgen Lake/Madison Valley display seasonality in Schuster tests; however, the variance tests indicate that events are randomly distributed.

Because of the possibility that seasonal variations in seismicity may be induced by external forcing at the ground surface [11,15,17,18], we use the same methodology to explore for seasonality in the upper 3 km of the crust only. If less than 50 earthquakes occur in the upper 3 km of the crust (as in the case of Mt. Hood and Lassen Peak), we use data from the upper 5 km. For each of the regions where we found convincing evidence of seasonal seismicity for both deep and shallow earthquakes, we found an equal or greater statistical significance in the

shallower portions of the crust. For 2- and 3-month groups, data from Mammoth Mountain, Hebgen Lake/Madison Valley, and Yellowstone Lake display seasonality (Table 2), indicating more focused periods of seasonality. In addition, data from the shallow crust at Hebgen Lake/Madison Valley suggest that seasonality there is statistically significant (p-values range from 0.03 to 0.09), with increased seismicity from June through December, depending on the statistical test (Table 2). Seasonality is also significant in 3-month groups and in three out of five tests in 2-month groups.

We calculated the power spectra for each region, using the complete data sets with daily binning. The power spectra of the full data set for the four volcanic areas with seasonal seismicity are shown in Fig. 4a. Only the data from Yellowstone Lake display a clear peak at a frequency of 365.25 days, although the Mammoth Mountain data set has a small peak at 384.47. Power spectra for the eastern south moat and Mt. St. Helens do not show evidence of annual cycles. We then calculated power spectra for seismic events in the top 3 km of the crust (Fig. 4b), which show stronger evidence

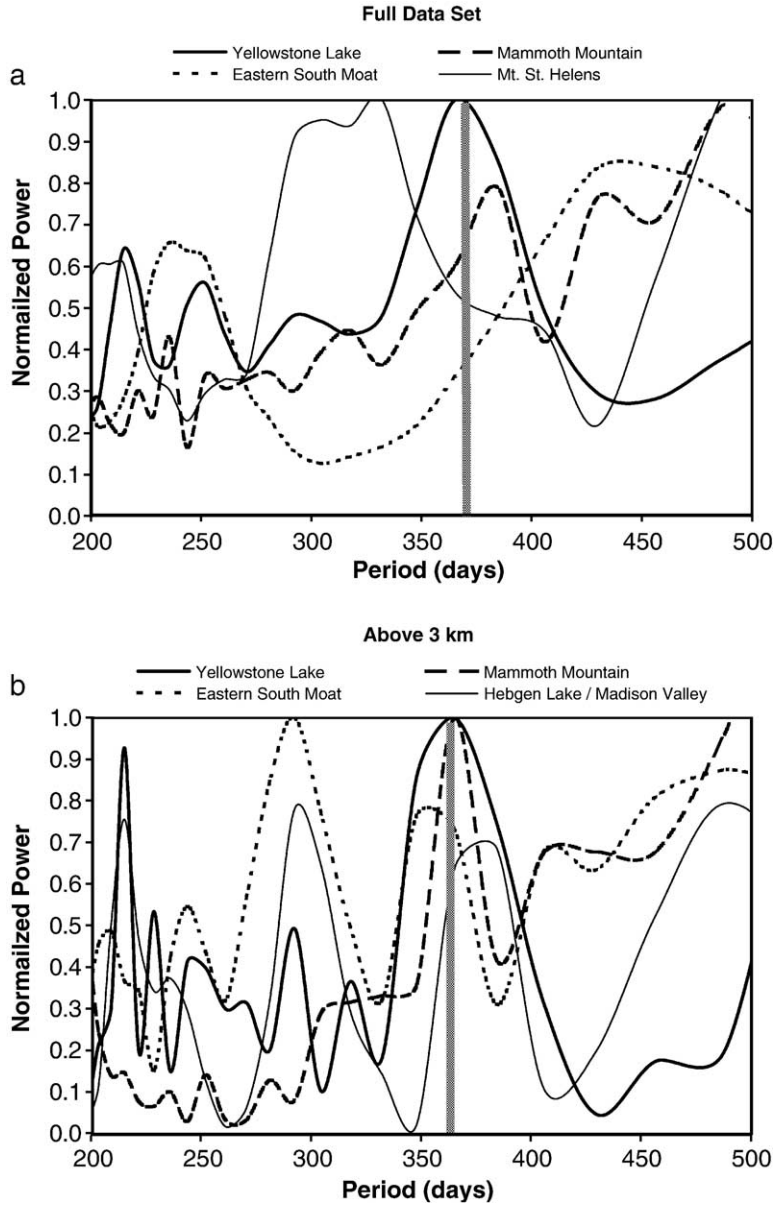

Fig. 4. Power spectra for regions that show increased monthly seismicity. (a) Full data set and (b) upper 3 km of the crust only. Vertical grey line denotes a period of 365.25 days.

for an annual period. The shallow data from both Yellowstone Lake and Mammoth Mountain show clearly defined peaks at 365.25 days, data from Hebgen Lake/Madison Valley have a small peak at 384.47, and data from the eastern south moat have a small peak at 347.86 (Fig. 4b). Data from Mt. St. Helens and the remaining volcanic areas show no distinguishable peaks and therefore are not represented in the figure. Although 20 yr of data is relatively short for calculating the power spectra of an annual period, evidence for seasonality is apparent in four of the regions.

5. Discussion

Significant annual periodicity in seismicity occurs in 4 of the 10 study regions (Table 1) and in 5 of 10 areas if only the upper 3 km of the crust are examined (Table 2). The timing of increased seismicity varies between locations and spans the whole year (Fig. 3). One region has increased seismicity during winter, helping to reaffirm that the results are not significantly affected by seismometer malfunctions during the winter months. Because seasonality appears to be common, we explore the possibility that external forces with annual frequencies might trigger seismicity.

Triggered earthquakes can be induced by changing the magnitude of stresses on faults. Earthquakes may be induced by an increase in the effective stress normal to a fault, a reduction in effective stress parallel to a fault, or equal decreases in effective stress in all principal directions. Mechanisms such as snow unloading, solid earth tides, and barometric pressure variations increase/decrease in stress in the vertical direction, whereas groundwater recharge reduces effective stress in all principal directions by increasing pore pressure. Previous studies of static stress change have concluded that, in most cases, static stress changes of less than 10 kPa are not sufficient to induce seismicity [37–39]. In laboratory experiments, a strong correlation between periodic stress and failure occurs at amplitudes of 50 to 100 kPa [40].

5.1. Snow unloading

Heki [15] suggested that unloading of snow on the western flanks of the Backbone Range in Japan triggers seasonal (spring–summer) earthquakes with $M>7$. Removal of the snow load (up to 10 kPa) in the spring may cause failure in shallow faults and initiate earthquakes. The vertical stress change at the surface during snow unloading is equal in magnitude and opposite in sign to the pressure created by the maximum snow load during mid-March through mid-May. Unloading should reduce vertical stress and unclamp normal faults, but should be less effective in triggering seismic activity on strike-slip faults. Most of the volcanic areas examined here are dominated by normal faults, but oblique and strike-slip faults are also present [21,29,41–43]. The faults at Mt. St. Helens are primarily strike-slip, as inferred from focal mechanisms [21].

In the Cascades, LVC, and Yellowstone, seismicity peaks at times ranging from less than 1 month to 6 months after timing of maximum snow load (Fig. 3). Stresses produced by the surface load propagate to seismogenic depths essentially instantaneously. The lag time between the onset of snow melt (unloading) and increased seismicity is not consistent with the crust behaving elastically, and may reflect a number of processes including: (1) variability in the response of crack growth to stress in the fault zone [35]; (2) the ability of fluids to reach crack tips and thus cause crack propagation [44,45]; (3) viscoelastic effects of the crust, affecting the fracture propagation [46]; and (4) longer nucleation time required for larger earthquakes, whereas smaller earthquakes may be modulated by shorter-term disturbances such as daily tides [15].

The average snow water equivalent (SWE) for April 1, historically the period of maximum snow accumulation, ranges from 0.5 to 1 m in the volcanic regions that have seasonal seismicity (http://cdec.water.ca.gov/snow/current/snow/; http://www.wcc.nrcs.usda.gov/snotel/). These loads result in a near-surface stress of 5–10 kPa. There is no snow load data in the eastern south moat so we use values at Mammoth Mountain as an approximation.

The total stress at the surface (e.g. the snow load), σ_t, is borne by both the pore fluid and the rock matrix, reducing the effective stress at seismogenic depths. The portion carried by pore fluid is determined by a tidal efficiency factor, α, which is dependent on bulk compressibility [47]:

$$\alpha = \frac{\beta_b}{\beta_b + \phi\beta_w} \tag{3}$$

where β_b is bulk compressibility of the porous medium, β_w is the compressibility of water, and φ is porosity. Thus the effective stress, σ_e, at depth is:

$$\sigma_e = \sigma_t - \alpha\sigma_t. \tag{4}$$

Assuming that bulk compressibility of volcanic rock ranges from 10^{-10} to 10^{-11} m^2/N, α is calculated to be 0.2 to 0.5. Given that seismogenic depths range from 2 to 8 km in the volcanic regions that have seasonality,

snow unloading may cause effective stress changes at seismogenic depths in the range of 1–6 kPa (Table 3, SWE load).

5.2. Groundwater recharge

Increases in pore fluid pressure caused by groundwater recharge can trigger seismicity by reducing the effective normal stress on faults. Unlike snow unloading, this process affects all fault types (normal, reverse, and strike-slip), because fluid pressure acts equally in all directions, independent of the stress tensor (e.g. [17]). Most groundwater recharge occurs during the spring as snowmelt infiltrates. The time required for the pressure pulse to diffuse from the surface to seismogenic depths, which is dependent on the hydraulic diffusivity and depth to the seismogenic zone, creates a lag time between peak recharge and peak seismicity.

The calculated pressure increase at the surface decays with depth, controlled by the hydraulic diffusivity and the depth to the region where seismicity occurs. Assuming that periodic groundwater recharge is in fact the cause of seasonal seismicity, a bulk hydraulic diffusivity can be calculated from the lag time, t, between peak recharge and peak seismicity [17]:

$$\kappa = \frac{\Psi z^2}{4\pi t^2} \tag{5}$$

where κ is hydraulic diffusivity, z is the depth of seismicity, and Ψ = is the period of the seasonal near-surface pore fluid pressure perturbation (1 yr).

To apply this equation, we assume that the medium is saturated from the surface to the depth of seismicity, and that the peak runoff time is June 1. The calculated hydraulic diffusivities range from 1.0 to 13.5 m^2/s in the volcanic areas with seasonality (Table 3). These calculated diffusivities are generally consistent with results of other studies in LVC and the Cascades [17,48–50]. The calculated hydraulic diffusivity at Hebgen Lake/Madison Valley is 1.5 m^2/s, generally consistent with seismic migration studies from that area that suggest values of 10 m^2/s [43].

The proportion of the near-surface pore-fluid pressure change that diffuses to a given depth is determined by the depth of seismicity and the hydraulic diffusivity [17]:

$$\frac{P'}{P_0} = \exp\left(-z\sqrt{\frac{\pi}{\Psi\kappa}}\right) \tag{6}$$

where P_0 and P' are the pressure changes near the surface and at depth, respectively. The amount of water table rise (e.g. the surface load) can be inferred from the SWE, the percent infiltration, and the porosity of the rock. For example, given an SWE of 1 m, 50% infiltration, and a rock porosity of 5%, the water table would rise 10 m. Because of the uncertainty in the percent infiltration and porosity, we calculate end-member possibilities for changes in the water table (20% porosity with 25% infiltration and 5% porosity with 50% infiltration). At LVC and Yellowstone Lake, more accurate estimates of the water-table variations are based on available well data (at LVC) and lake-level data (at Yellowstone Lake). The calculated water-table rise in the areas that have seasonality is 0.7–21 m, increasing the fluid pressure at the original water table by ~7–210 kPa (Table 3). Using the calculated hydraulic diffusivities, we calculate pressure changes of ~1–120 kPa at seismogenic depths (Table 3).

5.3. Barometric pressure

Annual barometric variations of 2 kPa have been proposed as a trigger for annual seismicity in LVC [11] and in the Philippines [16]. Mean annual barometric pressure variations of 2–4 kPa are similar to the ampli-

Table 3
Calculations of stress changes at seismogenic depths due to groundwater recharge and snow unloading for regions that have seasonal seismicity

Location	Depth (km)	SWE (m)	SWE load (kPa)	Lag (months)	κ (m^2/s)	P'/P_0 (%)	Δh (m)	ΔP_0 (kPa)	$\Delta P'$ (kPa)
Mt. St. Helens	3	0.9	2–5	1	3.4	0.7	1–9	11–90	8–64
Eastern south moat	8	1.1	2–6	5	1.0	0.1	1–3	10–29	1–2
Mammoth Mountain	6	1.1	2–6	1	13.5	0.6	3–21	29–206	18–123
Yellowstone Lake	5	0.5	1–3	1	9.3	0.6	0.7–2	7–20	4–12
Hebgen L./Madison V.	2	0.6	1–3	1	1.5	0.6	0.8–6	8–61	5–36

Calculations for Hebgen Lake/Madison Valley apply to the upper 3 km of the crust only. κ = hydraulic diffusivity, P'/P_0 = ratio of the pressure change at depth, P', to the pressure change in the near-surface, P_0, SWE = snow water equivalent, Δh = change in elevation of the water table due to complete melting of the SWE and associated groundwater recharge, assuming 25–50% infiltration and 5–20% porosity, ΔP_0 = change in pressure at the ground surface, $\Delta P'$ = calculated pressure at the seismogenic depth. SWE at the eastern south moat is based on data from Mammoth Mountain. Δh at LVC is based on well data and at Yellowstone Lake it is based on lake level.

tude of daily fluctuations (http://www.ncdc.noaa.gov/oa/ncdc.html). As with snow unloading, the total stress at the surface is partially carried by pore fluid. The change in effective stress at seismogenic depth is 0.4–2 kPa, which is likely insufficient to trigger earthquakes.

5.4. Solid earth tides

Daily earth tides with a strong ocean-load component have been inferred to modulate seismic activity at Pavlof volcano [12], Campi Flegrei [51], and the Juan de Fuca Ridge [13,14]. The amplitude of daily tidal variations exceeds 100 nanostrain at the systems examined here. Pole tides, caused by the wobbling of Earth's rotational axis, have 12- and 14-month periods. Forces exerted by these tides at the study areas, however, are relatively small, and peak-to-peak amplitudes are <3 nanostrain.

For a linear-elastic, homogeneous, isotropic material, the strain induced by annual tidal loading can be converted to stress using the relation $\sigma = E\varepsilon$, where σ is stress, E is Young's modulus, and ε is strain. Applying a Young's modulus of 70 GPa, stresses range from 0.1 to 0.2 kPa. These changes in pressure are likely insufficient to alter the stress regime; the change in pressure from annual tidal signals is <10–30% of other possible mechanisms.

5.5. Comparison of mechanisms

The stress changes induced by solid earth tides (<1 kPa) and barometric pressure variations (~2 kPa) are insufficient to have an effect on the seasonality of seismicity. Snow unloading and surface recharge generally create larger stress changes (Table 3). In most cases, groundwater recharge appears to be more significant. Snow unloading and groundwater recharge can both induce pressure changes at seismogenic depths of similar magnitude to the dynamic stresses inferred for remotely triggered earthquakes [3]. In the case of snow unloading, the change of stress at seismogenic depth appears to occur months before the period of elevated seismicity and we could potentially use this information to constrain the duration of earthquake nucleation and/or the viscous component of the mostly elastic upper crust [46]. The lag times are similar for Mammoth Mountain, Mt. St. Helens, Hebgen Lake/Madison Valley, and Yellowstone Lake (0.5–2.5 months). However, they are considerably longer at the eastern south moat (6 months). Increasing lag times do not correlate with increasing earthquake depth.

If snow unloading is the mechanism triggering seasonal earthquakes, one might expect a correlation between the number of earthquakes per year and the maximum SWE per year. We ranked the maximum yearly SWE and the number of earthquakes during the 6-month period of elevated monthly seismicity from 1 to 20 for the five regions that show seasonal seismicity, using only earthquakes from the upper 3 km

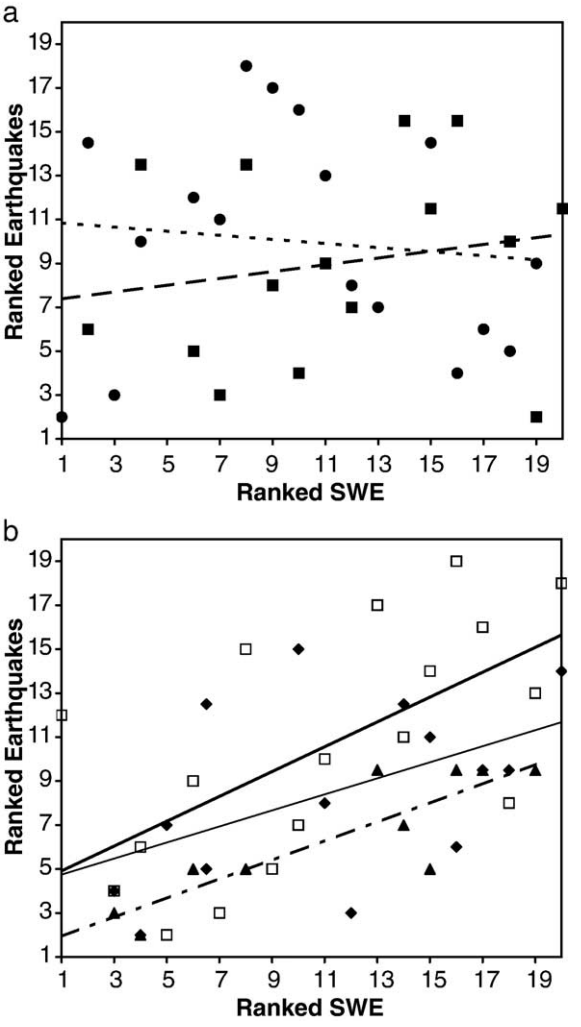

Fig. 5. Maximum SWE versus total number of earthquakes during the 6-month period of increased seismicity. Data are ranked from 1 to 20, based on the SWE and number of earthquakes, where 1 has the highest value. The highest ranking year and the lowest ranking year/years for the number of earthquakes are removed. Lines represent best fit to the data. (a) Regions with seasonality and little/no trend: circles, dotted line=eastern south moat, $R^2=0.01$; solid squares, dashed line=Mt. St. Helens, $R^2=0.04$. (b) Regions with seasonality and a stronger trend: diamonds, thin solid line=Yellowstone Lake, $R^2=0.24$; triangles, dot-dashed line=Hebgen Lake/Madison Valley, $R^2=0.75$; open squares, thick solid line=Mammoth Mountain, $R^2=0.39$.

of the crust for Hebgen Lake/Madison Valley. The year with the greatest number of earthquakes (ranked 1) was removed from the data set, because in most cases the number of earthquakes in this year was an order of magnitude larger than in the rest of the years, and likely related to magmatic or tectonic activity as opposed to external forcing. Similarly, we removed the lowest ranking year(s) and years with ≤1 earthquake because years with very low seismicity were indistinguishable. Although the data show considerable scatter, three of the five regions show a moderate correlation between years with increased seismicity and years with greater snow load (Fig. 5).

Groundwater recharge causes calculated stress increases at the depth of seismicity that are typically larger than those induced by snow unloading (Table 3). The interannual variability in groundwater recharge is likely correlated with SWE and could also explain the moderate correlation between number of earthquakes and the magnitude of SWE (Fig. 5). Further, diffusion of pore-fluid pressure changes can most readily explain the lag time between groundwater recharge and the onset of seismicity. Hydraulic diffusivities calculated from the lag times generally fall within the large range of values determined empirically and theoretically. Longer lag times, like those observed at the eastern south moat at LVC, imply low hydraulic diffusivity and very small pressure increases. In some cases, such as in the Cascade Range, the water table can be far below the land surface [52]. In such instances, water would first have to reach the water table before pore pressure diffusion can begin. Additionally, if the pore pressure gradient is sufficiently above hydrostatic, as may be expected in some volcanic environments, pore pressure will not diffuse to seismogenic depths efficiently.

The pressure change at depth is calculated from an exponential function (Eq. (5) substituted into Eq. (6)) based on lag time and the groundwater recharge load. Therefore, assuming pervasive faults at all depths, critical increases in earthquake triggering pressures are reached earlier and at shallower depths for larger pore-fluid pressure perturbations, P_0 [17]. This expected result conflicts with the actual timing of earthquakes observed in Mammoth Mountain, where earthquakes in the upper 3 km of the crust occur approximately 1 month later than those in the full seismic catalog. Perhaps this is due to the heterogeneity of hydraulic properties in the upper reaches of the crust. Elsewhere, increased seismicity in the uppermost crust either precedes or occurs simultaneously with seismicity in the full data set, as one would expect.

6. Conclusions

We examine 20-yr seismic records from 10 volcanically active areas in the western United States for seasonal seismicity. In order to examine annual trends, we use a variety of statistical tests on both the full data sets and subsets of the data. By comparing the results of variance tests, random walk tests, and power spectra, we find convincing evidence of annual trends in seismicity for five regions.

The data from 4 of the 10 studied areas show a statistical significance of ≥90% for seasonal seismicity

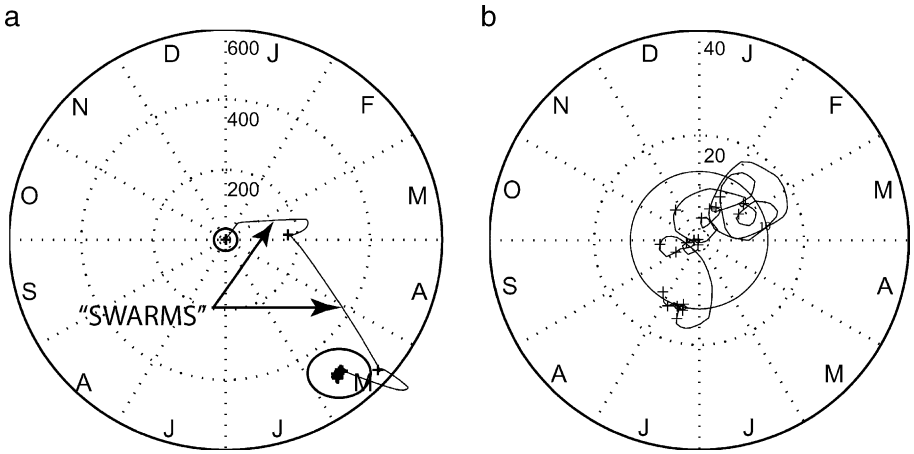

Fig. A1. (a) Schuster diagram for complete data set at Mt. St. Helens before deswarming. Letters designate the months of the year. "+" symbols indicate the first day of each year. Small circle in the center shows random walk radius for a nonrandom population distribution (R). Note that in the first 3 years, the number of earthquakes far exceeds the amount in subsequent years, as well as R. Arrows point to two swarm periods that are removed from the data set for subsequent Schuster tests. The region surrounded by an oval shows the activity in subsequent years, and is shown in figure b after swarm removal. (b) Remaining years of data after swarm removal. Solid circle shows circle with radius (R).

and data from 5 areas indicate a significance of ≥90% for seasonal seismicity in the upper 3 km of the crust. Four of those regions have pronounced annual peaks in power spectra for the upper 3 km of crust. In four of the five regions, seismicity peaks during the summer months, from approximately June through December. In the other region, increased seismicity occurs later in the year, from approximately November through April. In all cases, the cumulative seismic moment also increases during these periods.

We explored four possible triggering mechanisms for the observed seasonal seismicity. Both solid earth tides and barometric pressure variations cause changes in static stress of ≤2 kPa, likely insufficient to trigger seismicity. The static stress changes induced by snow unloading are as great as 5–6 kPa at Mt. St. Helens and LVC and somewhat lower at Yellowstone (1–3 kPa). Groundwater recharge may increase pore pressure at seismogenic depths by up to 120 kPa. Plausible values of hydraulic diffusivity, ranging from 1 to 13 m^2/s, are obtained from the apparent lag time between peak recharge and peak seismicity. For most regions showing seasonal seismicity, there is also a correlation between the magnitude of the SWE and the number of earthquakes in that year.

Acknowledgements

The authors would like to thank Nick Beeler, Dave Hill, Malcolm Johnston, Paul Reasenberg, Evelyn Roeloffs, and two anonymous reviewers for their constructive comments during the writing of this paper. We would also like to thank the National Research Council for funding for L.B. Christiansen. Funding for this research came from the USGS Volcano Hazards Program.

Appendix A

Schuster tests often reveal that one or more years of seismic data dominate the random walk pattern, indicating elevated seismic activity as compared to more typical years (Fig. A1a). The high-seismicity periods, likely caused by either magma intrusions or tectonic activity and unrelated to seasonal patterns, are classified as swarm periods. We define a swarm period as any single year in which the Schuster Random Walk exceeds the average walkout length (***R***). This length, ***R***, is dependent on the number of events in the time series; as the length of the time series increases, ***R*** increases, which classifies less seismic sequences as earthquake swarms. However, with a longer time series, each year has a smaller effect on the overall distribution and therefore would not cause as severe a bias to the analysis results. In order to maintain a continuous time series, we remove a complete year of data surrounding the swarm period for the Schuster test analyses only. We determine the start and end dates of the excised year by establishing the day on which most seismic activity occurs and then removing half a year of data before and after that day. We use full data sets in determining minimum magnitude cutoffs and swarm periods. We then retest the reduced data sets using Schuster tests to quantify annual seasonal seismicity (Fig. A1b). The south moat of LVC experiences swarm sequences almost yearly. Other areas also exhibit relatively frequent, non-seasonal swarm sequences.

References

[1] D.P. Hill, P.A. Reasenberg, A.J. Michael, W.J. Arabasz, G.C. Beroza, D.S. Brumbaugh, J.N. Brune, R. Castro, S.D. Davis, D.M. dePolo, W.L. Ellsworth, J.S. Gomberg, S.C. Harmsen, L. House, S.M. Jackson, M.J.S. Johnston, L.M. Jones, R. Keller, S.D. Malone, L. Munguia, S. Nava, J.C. Pechmann, A.R. Sanford, R.W. Simpson, R.B. Smith, M.A. Stark, M.C. Stickney, A. Vidal, S.R. Walter, V. Wong, J.E. Zollweg, Seismicity remotely triggered by the magnitude 7.3 Landers, California, earthquake, Science 260 (1993) 1617–1623.

[2] S. Husen, R. Taylor, R.B. Smith, H. Healser, Changes in geyser eruption behavior and remotely triggered seismicity in Yellowstone National Park produced by the 2002 M 7.9 Denali Fault earthquake, Alaska, Geology 32 (2004) 537–540.

[3] S.G. Prejean, D.P. Hill, E.E. Brodsky, S.E. Hough, M.J.S. Johnston, S.D. Malone, D.H. Oppenheimer, A.M. Pitt, K.B. Richards-Dinger, Remotely triggered seismicity on the United States west coast following the Mw 7.9 Denali fault earthquake, Bull. Seismol. Soc. Am. 94 (2004) S348–S359.

[4] E.E. Brodsky, B. Sturtevant, H. Kanamori, Earthquakes, volcanoes, and rectified diffusion, J. Geophys. Res. 103 (1998) 23827–23838.

[5] J. Gomberg, N.M. Beeler, M.L. Blanpied, P. Bodin, Earthquake triggering by transient and static deformation, J. Geophys. Res. 103 (1998) 24411–424426.

[6] D.P. Hill, F. Pollitz, C. Newhall, Earthquake–volcano interactions, Phys. Today 55 (2002) 41–47.

[7] A.T. Linde, I.S. Sacks, M.J.S. Johnston, D.P. Hill, R.G. Bilham, Increased pressure from rising bubbles as a mechanism for remotely triggered seismicity, Nature 371 (1994) 408–410.

[8] E.E. Brodsky, E. Roeloffs, D. Woodcock, I. Gall, M. Manga, A mechanism for sustained groundwater pressure changes induced by distant earthquakes, J. Geophys. Res. 108 (2003), doi:10.1029/2002JB002321.

[9] D.P. Hill, J.O. Langbein, S. Prejean, Relations between seismicity and deformation during unrest in Long Valley Caldera, California, from 1995 through 1999, J. Volcanol. Geotherm. Res. 127 (2003) 175–193.

[10] M.J.S. Johnston, D.P. Hill, A.T. Linde, J. Langbein, R. Bilham, Transient deformation during triggered seismicity from the June 28, 1992, *Mw* = 7.3 Landers earthquake at Long Valley volcanic caldera California, Bull. Seismol. Soc. Am. 85 (1995) 787–795.

[11] S.S. Gao, P.G. Silver, A.T. Linde, I.S. Sacks, Annual modulation of triggered seismicity following the 1992 Landers earthquake in California, Nature 406 (2000) 500–504.
[12] S.R. McNutt, R.J. Beavan, Volcanic earthquakes at Pavlof volcano correlated with solid earth tide, Nature 294 (1981) 615–618.
[13] M. Tolstoy, F.L. Vernon, J.A. Orcutt, F.K. Wyatt, Breathing of the seafloor; tidal correlations of seismicity at Axial Volcano, Geology 30 (2002) 503–506.
[14] W.S.D. Wilcock, Tidal triggering of microearthquakes on the Juan de Fuca Ridge, Geophys. Res. Lett. 28 (2001) 3999–4002.
[15] K. Heki, Snow load and seasonal variation of earthquake occurrence in Japan, Earth Planet. Sci. Lett. 207 (2003) 159–164.
[16] M. Ohtake, H. Nakahara, Seasonality of great earthquake occurrence at the northwestern margin of the Philippine Sea Plate, Pure Appl. Geophys. 155 (1999) 689–700.
[17] M.O. Saar, M. Manga, Seismicity induced by seasonal groundwater recharge at Mt. Hood, Oregon, Earth Planet. Sci. Lett. 214 (2003) 605–618.
[18] L.W. Wolf, C.A. Rowe, R.B. Horner, Periodic seismicity near Mt. Ogden on the Alaska–British Columbia border; a case for hydrologically triggered earthquakes? Bull. Seismol. Soc. Am. 87 (1997) 1473–1483.
[19] J.B. Adams, M.E. Mann, C.M. Ammann, Proxy evidence for an El Nino-like response to volcanic forcing, Nature 426 (2003) 274–278.
[20] B.G. Mason, D.M. Pyle, W.B. Dade, T. Jupp, Seasonality of volcanic eruptions, J. Geophys. Res. 109 (2004), doi:10.1029/2002JB002293.
[21] S.C. Moran, Seismicity at Mount St. Helens, 1987–1992: evidence for repressuring of an active magmatic system, J. Geophys. Res. 99 (1994) 4341–4354.
[22] S.C. Moran, J.M. Lees, S.D. Malone, *P* wave crustal velocity structure in the greater Mt. Rainier area from local earthquake tomography, J. Geophys. Res. 104 (1999) 10775–710786.
[23] R.D. Norris, C.S. Weaver, K.L. Meagher, A. Qamarer, R.J. Blakely, Earthquake swarms at Mount Hood; relation to geologic structure, Seismol. Res. Lett. 70 (1999) 218.
[24] S.R. Walter, Ten years of earthquakes at Lassen Peak, Mount Shasta, and Medicine Lake volcanoes, Northern California; 1981–1990, Seismol. Res. Lett. 62 (1991) 25.
[25] D.P. Hill, R.A. Bailey, A.S. Ryall, Active tectonic and magmatic processes beneath Long Valley Caldera, eastern California; an overview, J. Geophys. Res. 90 (1985) 11111–111120.
[26] R.A. Bailey, G.B. Dalrymple, M.A. Lanphere, Volcanism, structure, and geochronology of Long Valley Caldera, Mono County, California, J. Geophys. Res. 81 (1976) 725–744.
[27] M.L. Sorey, Evolution and present state of the hydrothermal system in Long Valley Caldera, J. Geophys. Res. 90 (1985) 11219–211228.
[28] R.L. Christiansen, The Quaternary and Pliocene Yellowstone Plateau volcanic field of Wyoming, Idaho, and Montana, U. S. Geol. Surv. Prof. Pap. (2001) G1–G145.
[29] G.P. Waite, R.B. Smith, Seismotectonics and stress field of the Yellowstone volcanic plateau from earthquake first-motions and other indicators, J. Geophys. Res. 109 (2004), doi:10.1029/2003JB002675.
[30] D.I. Doser, Source parameters and faulting processes of the 1959 Hebgen Lake, Montana, earthquake sequence, J. Geophys. Res. 90 (1985) 4537–4555.
[31] L.A. Morgan, W.C. Shanks III, D.A. Lovalvo, S.Y. Johnson, W.J. Stephenson, K.L. Pierce, S.S. Harlan, C.A. Finn, G. Lee, M. Webring, B. Schulze, J. Duehn, R.E. Sweeney, L.S. Balistrieri, Exploration and discovery in Yellowstone Lake; results from high-resolution sonar imaging, seismic reflection profiling, and submersible studies, J. Volcanol. Geotherm. Res. 122 (2003) 221–242.
[32] W.J. Dixon, J.F.J. Massey, Introduction to Statistical Analysis, McGraw-Hill Book Company, New York, 1983. 678 pp.
[33] A. Schuster, On lunar and solar periodicities of earthquakes, Proc. R. Soc. Lond. 61 (1897) 455–465.
[34] P.A. Rydelek, L. Hass, On estimating the amount of blasts in seismic catalogs with Schuster's Method, Bull. Seismol. Soc. Am. 84 (1994) 1256–1259.
[35] N.M. Beeler, D.A. Lockner, Why earthquakes correlate weakly with the solid Earth tides: effects of periodic stress on the rate and probability of earthquake occurrence, J. Geophys. Res. 108 (2003) , doi:10.1029/2001JB001518.
[36] E.S. Cochran, J.E. Vidale, S. Tanaka, Earth tides can trigger shallow thrust fault earthquakes, Science 306 (2004) 1164–1166.
[37] J.L. Hardebeck, J.J. Nazareth, E. Hauksson, The static stress change triggering model; constraints from two Southern California aftershock sequences, J. Geophys. Res. 103 (1998) 24427–424437.
[38] P.A. Reasenberg, R.W. Simpson, Response of regional seismicity to the static stress change produced by the Loma Prieta earthquake, Science 255 (1992) 1687–1690.
[39] R.W. Simpson, P.A. Reasenberg, Earthquake-induced static-stress changes on Central California faults, U. S. Geol. Surv. Prof. Pap. (1994) F55–F89.
[40] D.A. Lockner, N.M. Beeler, Premonitory slip and tidal triggering of earthquakes, J. Geophys. Res., B, Solid Earth Planets 104 (1999) 20133–120151.
[41] J. Jones, S.D. Malone, Constraints on Mt. Hood earthquake swarms from cross-correlation and joint hypocenter determination, Seismol. Res. Lett. 73 (2002) 253.
[42] L.J.P. Muffler, M.A. Clynne, D.E. Champion, Late Quaternary normal faulting of the Hat Creek Basalt, northern California, Geol. Soc. Amer. Bull. 106 (1994) 195–200.
[43] G.P. Waite, R.B. Smith, Seismic evidence for fluid migration accompanying subsidence of the Yellowstone Caldera, J. Geophys. Res. 107 (9) (2002) 13.
[44] R.J. Martin III, Time-dependent crack growth in quartz and its application to the creep of rocks, J. Geophys. Res. 77 (1972) 1406–1419.
[45] R.J. Martin III, W.B. Durham, Mechanisms of crack growth in quartz, J. Geophys. Res. 80 (1975) 4837–4844.
[46] A.M. Jellinek, M. Manga, M.O. Saar, Did melting glaciers cause volcanic eruptions in eastern California? Probing the mechanics of dike formation, J. Geophys. Res. (2004), doi:10.1029/2004JB002978.
[47] P.A. Domenico, F.W. Schwatrz, Physical and Chemical Hydrogeology, John Wiley & Sons, Inc., New York, 1990. 506 pp.
[48] E. Roeloffs, M. Sneed, D.L. Galloway, M.L. Sorey, C.D. Farrar, J.F. Howle, J. Huges, Water-level changes induced by local and distant earthquakes at Long Valley caldera, California, J. Volcanol. Geotherm. Res. 127 (2003) 269–303.
[49] S.A. Rojstaczer, Intermediate period response of water levels in wells to crustal strain; sensitivity and noise level, J. Geophys. Res. 93 (1988) 13619–613634.

[50] M.O. Saar, M. Manga, Depth dependence of permeability in the Oregon Cascades inferred from hydrogeologic, thermal, seismic, and magmatic modeling constraints, J. Geophys. Res. 109 (2004), doi:10.1029/2003JB002855.

[51] P.A. Rydelek, I.S. Sacks, R. Scarpa, On tidal triggering of earthquakes at Campi Flegrei, Italy, Geophys. J. Int. 109 (1992) 125–137.

[52] S. Hurwitz, K.L. Kipp, M.E. Reid, S.E. Ingebritsen, Groundwater flow, heat transport, and water-table position within volcanic edifices: implications for volcanic processes in the Cascade Range, J. Geophys. Res. (2003), doi:10.1029/2003JB002565.